ACS OMEGA

Open Access

http://pubs.acs.org/journal/acsodf

Article

Molybdenum Disulfide Nanosheet-Based Nanocomposite for the Topical Delivery of Umbelliferone: Evaluation of Anti-inflammatory and Analgesic Potentials

Diwya Kumar Lal, Bhavna Kumar,* Vishakha Kaushik, Adel Alhowyan, and Mohd Abul Kalam

Cite This: *ACS Omega* 2024, 9, 37105−37116

Read Online

ACCESS | Metrics & More | Article Recommendations | Supporting Information

ABSTRACT: This study aimed to develop a nanocomposite formulation comprising umbelliferone (UMB) and molybdenum disulfide (MoS_2) nanosheets as a carrier, termed as the UMB−MoS_2 nanocomposite in gel for topical delivery. MoS_2 nanosheets were successfully synthesized via a green-hydrothermal reaction of 10 mg of ammonium molybdate and 10 mg of thiourea in 80 mL of deionized water under predetermined conditions. The UMB−MoS_2 nanocomposite was prepared by sonicating UMB and MoS_2 nanosheets (each of 1 mg/mL) in dimethylformamide. Scanning electron microscopy revealed crumpled nanosheets with an open-ended structure and a nanocomposite as a layered structure. The X-ray diffraction pattern revealed the amorphous nature of UMB in the UMB−MoS_2 nanocomposite. Fourier-transform infrared spectra of the UMB−MoS_2 nanocomposite had modified bands of the functional group, which confirmed the formation of the nanocomposite. The size and polydispersity-index (435 nm and 0.415, respectively) of the nanocomposite were within the limit for an efficient topical application. Carbopol 934 (2%) was used to prepare the UMB−MoS_2 nanocomposite gel (F1) and UMB-Carbopol gel (F2, for comparative evaluation). The pH, spreadability, and viscosity of F1 were found to be 5.56, 5.89 g·cm/s, and 32.5 Pa-sec, respectively, which were optimal for the topical application of gel-based formulations. In vitro release characteristics of both formulations were deemed to be suitable for topical application, where F1 exhibited a biphasic drug release profile and a superior release rate of 94.8% compared to 43.5% for F2 at 24 h. In the carrageenan-induced rat paw edema model, the animal group treated with F1 demonstrated the lowest increase in paw thickness of 26.6%, which was significantly lower as compared to the F2-treated group (52.9%) and the diclofenac sodium-treated group (32.2%). Similarly, in the tail immersion method, F1 exhibited the highest peak tail withdrawal latency of 10.9 s, significantly greater than F2 (8.9 s) and standard treatment (10 s), indicating the superior analgesic activity of F1. This pioneering work introduces a novel UMB−MoS_2 nanocomposite with promising anti-inflammatory and analgesic potentials, paving the way for further research into the biomedical applications of MoS_2-based nanocarriers.

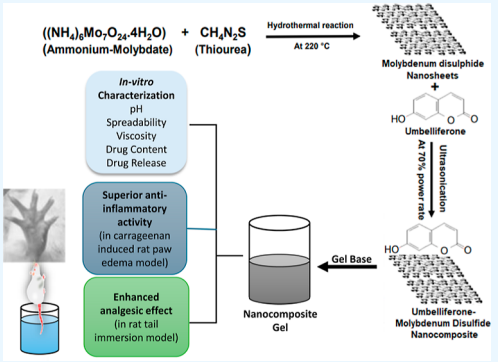

1. INTRODUCTION

Inflammation acts as a dynamic protective response when our body faces threats from external factors, internal cell damage, or infections. It triggers the release of immune mediators, leukocytes, or chemokine in the affected region. This process helps remove harmful substances and promote the healing of the affected tissue.[1] However, excessive inflammation damages healthy tissues, leading to chronic inflammation. This persistent inflammation is linked to the development of various skin conditions, including dermatitis (atopic, contact, and seborrheic), eczema, psoriasis, and rosacea.[2−5] Most of the drugs used to treat inflammation possess significant side effects, especially those related to the gastrointestinal tract such as for long-term use of NSAIDs and steroids.[6] Therefore, more research is being done to look for alternatives.

Coumarins such as umbelliferone (UMB) are a potent alternative, with no reported toxicity in mammalian systems as far as literature reports.[7] UMB (chemically 7-hydroxycoumarin) is a major biotransformed outcome of coumarins. It is widely distributed in several number plants, particularly in families of *Apiaceae* (*Umbelliferae*), *Rutaceae*, and *Asteraceae*.[8,9] UMB exhibits potent anti-inflammatory and antioxidant action along with antidiabetic, anticancer, antiarthritic, antiallergic, and liver protective effects.[10,11] UMB exerts anti-inflammatory action by inhibiting both the central and peripheral pain mediators.[12] UMB blocks the biosynthesis of prostaglandin involving hydroxy and epoxy fatty acids in arachidonic acid cascade, demonstrating that it works in a way that is comparable to NSAIDs.[7] Additionally, it possesses a dose-

Received: May 3, 2024
Revised: August 12, 2024
Accepted: August 13, 2024
Published: August 20, 2024

dependent antioxidative effect that assists in ameliorating the inflammation[13] and reported to have potential therapeutic action against atopic dermatitis.[11] However, the limited water solubility restricts its use as an anti-inflammatory drug.[14]

Molybdenum disulfide (MoS_2) is a 2D layered transition metal dichalcogenide nanomaterial and has potential for drug delivery nanocarriers owing to its intercalated nature, biocompatibility, and high loading capabilities.[15] The 2D layers are stacked due to van der Waals forces, and layers are held together by strong covalent bonds between atoms.[16] As per the safety data sheet by ACS Material LCC (USA), MoS_2 is a crystalline, nonfibrous, and synthetic material which is not hazardous.[17] Moreover, previous toxicity investigation of MoS_2 during the patch testing on guinea pigs to assess potential allergic reactions after topical application did not reveal any concerning allergic responses.[18] Because of lower toxicity compared to graphene oxide, the transition-metal dichalcogenides such as MoS_2, WS_2, and WSe_2 have been studied for potential use in hepatocellular carcinoma and a variety of biomedical research.[19] The outstanding photothermal conversion capability of MoS_2 in the near-infrared region leads to its extensive biomedical applications. MoS_2 nanostructures with DNA oligonucleotides played a double role of protection and delivery as well as contributed an increased stimuli-sensitive drug delivery carrier for many targeted chemotherapies.[20] Folic acid-grafted bovine serum albumin-functionalized MoS_2 was explored for the targeted treatment of folic acid-receptor positive breast cancers.[21] Several studies have investigated the role of MoS_2 as a drug carrier majorly for cancer[22,23] along with few research studies on inflammatory conditions such as osteoarthritis and spinal cord injuries.[15,24] The abundance of unsaturated Mo and S sites on the outer layer of MoS_2 causing substantial interactions with cells can be particularly effective in topical delivery of anti-inflammatory drugs as it may lead to local effect, prolong drug retention, and enhanced absorption. Additionally, MoS_2 itself can ameliorate inflammation via MoS_2-mediated anti-inflammatory macrophage modulations improving the overall outcome of the treatment.[15] These investigations notwithstanding, there has not been a lot of work done on employing MoS_2 for drug delivery.

This study reports the pioneering use of MoS_2 nanosheets as a nanocarrier for the topical delivery of UMB for dermal application. In this study, the MoS_2 nanosheets were synthesized at low temperature, and then, a novel UMB−MoS_2 nanocomposite was prepared using the sonication method for the effective delivery of UMB. Here, MoS_2 was intended to be used as a drug carrier having anti-inflammatory property to access the synergistic action alongside UMB. To confirm the formation of the nanocomposite, Fourier-transform infrared (FTIR) spectroscopy and powder X-ray diffraction (pXRD) have been employed. Finally, the UMB−MoS_2 nanocomposite gel has been formulated and assessed for different in vitro and in vivo experiments. This approach of combination may provide insights into the role of MoS_2 with other bioactives for other biomedical applications.

2. MATERIALS AND METHODS

2.1. Materials. UMB ($C_9H_6O_3$; MW: 162.14 g/mol) was purchased from "Dhamtec Pharma and Consultants, Mumbai, India" with >98.0% purity by gas chromatography. The ammonium-molybdate [$(NH_4)_6Mo_7O_{24}{\cdot}4H_2O$], thiourea ($CH_4N_2S$), Carbopol 934, potassium dihydrogen phosphate (KH_2PO_4), and methanol were purchased from SD Fine Chemicals, Mumbai, India. Carrageenan (a sulfated polysaccharide), anhydrous *N*,*N*-dimethylformamide [(DMF), purity ≥99.8%], and ethanol (absolute) were purchased from Sigma-Aldrich Co. Ltd. (St. Louis, MO, USA), now owned by MERCK, Darmstadt, Germany. 2-diphenyl-1-picrylhydrazyl (DPPH) and NaCl were bought from HiMedia Laboratories Pvt. Ltd., Maharashtra, India. Purified water (Milli-Q) was obtained in-house by a filter unit (Millipore, Molsheim, France). All other analytical grade chemicals and reagents were used as received without further purification.

2.2. Methods. *2.2.1. Synthesis of MoS_2 Nanosheets.* The MoS_2 nanosheets were synthesized by a simple one-step hydrothermal method using ammonium-molybdate [$(NH_4)_6Mo_7O_{24}{\cdot}4H_2O$] and thiourea ($CH_4N_2S$) as the precursors.[25] Both materials (10 mg each) were mixed with 80 mL of deionized water using a magnetic stirrer (400 rpm) at 25 °C. The prepared dispersion was put into a 250 mL stainless steel autoclave that had a high temperature and corrosion-resistant polytetrafluoroethylene Teflon liner. The autoclave is kept inside an oven at 220 °C for 8 h. The prepared powder samples were washed and cleaned using water and ethanol several times and dried using a vacuum oven for 12 h at 60 °C.[26]

2.2.2. Preparation of a UMB−MoS_2 Nanocomposite. The UMB−MoS_2 nanocomposite was prepared by adopting and slightly modifying the previously reported methods.[27,28] An accurately weighed amount of UMB (10 mg) was dissolved in 10 mL of DMF under moderate magnetic stirring (400 rpm) to get 1 mg/mL solution of UMB. Separately, MoS_2 (10 mg) was also dissolved in DMF (10 mL) to make MoS_2 solution of 1 mg/mL concentration. Both solutions were sonicated individually for 20 min. UMB solution was added dropwise to the MoS_2 solution under ultrasonication at 45 °C for 30 min. The resulting solution was further sonicated in three cycles of 15 min. It was further sonicated using a probe sonicator for 10 min at 70% power rate. The obtained solution was further centrifuged at 12,000 rpm and 10 °C for 15 min. The precipitated nanocomposite was collected and dried at 80 °C for 4 h in an oven.

2.2.3. Preparation of UMB−MoS_2 Nanocomposite Gel. An aqueous solution of 2% (w/v) Carbopol 934 was prepared and was left overnight for complete swelling of the gel base and then mixed with 1% (v/v) of glycerol. Thereafter, the UMB−MoS_2 nanocomposite was dispersed in ethanol followed by 2 min of vortexing. The solution was mixed with the Carbopol 934 gel base under magnetic stirring (400 rpm) for 30 min. The pH of the UMB−MoS_2 nanocomposite gel (F1) was adjusted between 5.5 and 6.5 with triethanolamine and stored in a suitable environment until further use. Similarly, for comparative study, the conventional gel containing pure UMB (F2) was prepared by directly dissolving UMB in ethanol and incorporating the solution in Carbopol 934 gel base (F2). The prepared gels were kept untouched for 10−12 h to get rid of entrapped air bubbles (if any).

2.3. Characterization of the MoS_2 Nanosheets and MoS_2−UMB Composite. *2.3.1. Surface Morphology by Scanning and Transmission Electron Microscopy.* The morphology of the nanocomposite was examined by using scanning electron microscopy (SEM). The SEM generates an image by sensing secondary or backscattered electrons producing 3D images, providing information on the sample's surface and its composition. On the copper grid encased by a

https://doi.org/10.1021/acsomega.4c04252
ACS Omega 2024, 9, 37105−37116

carbon film, a drop of the appropriately diluted nanocomposite suspension was applied and dried. To lessen the impacts of sample charging due to electron beam, a thin layer (3.5 nm) of gold-coating was done on the surface of samples using gold-sputtering. The SEM images of the nanocomposite samples were obtained using Hitachi S3800 SEM (Hitachi, Japan) operating at 0.2−10 kV accelerating voltage and up to 1000-times magnifications.[29,30]

Aqueous diluted (with purified water at 1/10, v/v) F1 (40 μL) was put on a copper grip and air-dried. Then, 1% phosphotungstic acid (40 μL) was poured on the dried sample. The sample on the grid was left untouched to settle down for a few minutes. The excess sample (if any) was wiped by filter paper, and the grid was kept at 25 ± 1 °C for 2−3 h to get dried before scanning by transmission electron microscopy (TEM; FEI, Tecnai G2 20 Twin, the Netherlands). TEM was operated at 200 kV to capture the image at 20,000-times of magnifications.[31]

2.3.2. Powder X-ray Diffraction. Using pXRD (XPERT-PRO Diffractometer, PANalytical, the Netherlands), the crystallinity and phase purity of the MoS_2, UMB, and nanocomposites were assessed having a CuKα radiation source (λ = 0.15406 nm, 45 kV and 40 mA) at 25 °C.[32]

2.3.32.3.3. Fourier-Transform Infrared Spectroscopy. FTIR spectroscopy (IRAffinity-1S, Shimadzu, Kyoto, Japan) was used to validate the formation of the nanocomposite. Samples were analyzed between the resolution of 4000 and 400 cm^{-1}.[33]

2.3.4. Particle Size and Polydispersity-Index. The particle size analysis defines the dimensions and reveals the size of the prepared nanocomposites, while polydispersity-index relates to the uniformity in particle size and their distribution throughout the sample. The samples were sufficiently diluted with ultrapure water to prevent multiple scattering. Zetasizer Nano-Series (Malvern Ltd.) was used to check the size and polydispersity index (PDI) of the developed formulation. The He−Ne laser's intensity at a wavelength of 633 nm was evaluated while positioned at the scattering angle of 90° and maintained at 25 °C temperature.[32−34]

2.3.5. Percentage Yield. The percentage (%) yield indicates the efficacy of the process of synthesis of the UMB−MoS_2 nanocomposite. It was performed in triplicate and was calculated by the following expression (eq 1)

$$\text{yield (\%)} = \frac{\text{practical yield (weight of prepared sample)}}{\text{theoretical yield (total weight of drug and excipients)}} \times 100 \quad (1)$$

2.4. Determination of pH, Spreadability, Viscosity, and Drug Content for UMB−MoS_2 Nanocomposite-Containing Gel. For topical delivery, pH is an important parameter to be analyzed, indicating the formulation's acidity or basicity. The formulation should have a pH range of 4 with the skin's pH.[35] The pH of the gel was determined by immersing the electrode of a calibrated digital pH meter (LT-11, Labtronics, India) in triplicate.

Spreadability corresponds to the ability of the gel to spread across the skin. Good spreadability property helps in the even distribution of the gel, thus affecting the therapeutic efficacy of the formulation. The parallel plate method was employed to determine the spreadability of the gel. Briefly, 500 g of gel was put on the glass slab inside a premarked 1 cm circle. The other glass slide was placed above it onto which 500 g weight was put and the increase in the diameter (cm) was noted.[36] The following expression (eq 2) was used for the determination of spreadability

$$\text{spreadability} = \frac{(\text{final diameter} - \text{initial diameter})}{\text{time}} \times \text{mass placed on upper slide} \quad (2)$$

Viscosity simply represents the consistency of the formulation. It governs various parameters like spreadability, skin retention, drug release, etc. Being a non-Newtonian fluid, the viscosity of gel changes with change in applied shear rate, thus the viscosity was determined over a range of 10−250 s^{-1} shear rate and at 25 °C.[37] An easy and quick rheological measurement (viscosity) of the samples was performed by a modular compact rheometer (MCR)-series (Model MCR-72, Anton Paar, Austria).

Drug content determines the drug distribution within the gel, signified by the percentage of drug incorporated within the gel. It was determined by dissolving 1 g of gel in 10 mL of methanol with continuous magnetic stirring for 1 h and determining the amount of drug by the UV-spectroscopic method at a wavelength of 324 nm.[38,39] The drug content (%) was calculated as per the following expression (eq 3).

$$\text{drug content (\%)} = \frac{\text{drug amount detected by UV}}{\text{theoretical amount of drug}} \times 100 \quad (3)$$

2.5. In Vitro Drug Release Study. The in vitro release study was conducted using a Franz diffusion cell using a dialysis membrane (Fisherbrand regenerated Cellulose Dialysis Tubing, Fisher Scientific) having MWCO: 12−14 kDa, as a release barrier. The dialysis membrane was activated, keeping it in glycerin overnight, and was hydrated by washing and putting it in "phosphate buffer saline (PBS, pH 7.4)" for 30 min. One gram (1 g) of each, the UMB−MoS_2 nanocomposite gel (F1) and UMB containing conventional gel (F2) were placed inside donor compartments of different cells. Each formulation was containing approximately ≈5 mg of UMB. The PBS (pH 7.4) was poured into the receiver chamber and was maintained at 37 ± 0.5 °C with constant stirring at 50 rpm. Aliquots of 1 mL were withdrawn at predetermined time points, and the same amount of fresh release medium (PBS, pH 7.4) was replaced after each withdrawal. The withdrawn samples were analyzed using a UV−visible spectrophotometer (Shimadzu, Japan) at a wavelength of 324 nm.[38,39] The experiment was performed in triplicate for both the formulations. Drug release data was fitted into release kinetic models to determine the mechanism of drug release from the formulation.[40]

2.6. Bioadhesive Strength. Bioadhesive strength refers to the capacity of a formulation to adhere to biological surfaces. Fresh rat skin was obtained and prepared by removing excess fat and rinsing it with physiological saline solution. Two rat skin samples of identical size (1.5 × 1.5 cm) were carefully mounted onto the lower side of a balance pan and a wooden box in a modified bioadhesion measuring apparatus. To secure their position during the test, a cyanoacrylate adhesive was used. Around 100 mg of F1 was placed on the skin surfaces and was pressed against each other for 1 min to ensure proper adhesion and to remove any air present between them. Water was added dropwise to the other side of the pan. The weight of water at which two skin layers separated was noted, and the bioadhesive strength of the formulation was calculated using eq 4[41,42].

https://doi.org/10.1021/acsomega.4c04252
ACS Omega 2024, 9, 37105−37116

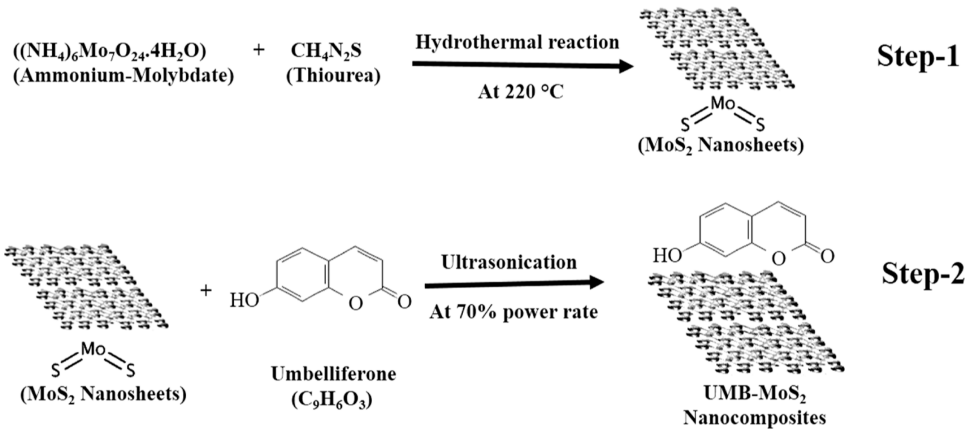

Figure 1. Schematic representation of the stepwise synthesis of MoS_2 nanosheets (Step-1) and the formulation of UMB−MoS_2 nanocomposites (Step-2).

$$\text{Bioadhesive strength} = \frac{\text{weight of water} \times \text{gravitational acceleration}}{\text{area of skin sample}} \quad (4)$$

2.7. In Vivo Animal Study. White albino rats weighing 200−250 g were used in this study. The ethical clearance was obtained from the Institutional Ethics Committee (Ethics Approval no.: DITU/IAEC/22/4/13). The rats were divided into four different groups with six rats (n = 6) per group assigned for the specific treatment. Group-I served as the control (received Carbopol 934 gel without UMB), Group-II was the treatment group (with UMB-loaded Carbopol 934 gel), Group-III also served as the treatment group (with UMB-MoS_2 nanocomposite-loaded Carbopol 934 gel), and Group-IV was the positive control or standard group, treated with diclofenac emulgel.

2.7.1. Anti-inflammatory Activity. In vivo anti-inflammatory study was carried out using the carrageenan-induced rat paw edema method. Before the experiment, the animals were fasted overnight but were given unlimited access to water. Around 400 mg of gel (≈4 mg of UMB−MoS_2 nanocomposite ≈ to 2 mg of UMB) from the assigned treatments, including UMB−MoS_2 nanocomposite loaded gel (F1), UMB (2 mg) containing conventional Carbopol 934 gel (F2), placebo gel (Carbopol 934 gel without UMB), and 100 mg of standard (diclofenac emulgel, equivalent to 2 mg of diclofenac sodium), was topically applied to the paws of the respective groups of rats 30 min prior to carrageenan injection. The weighed amount of gels was applied and rubbed uniformly on the paw of each rat. After applying the dosage forms, the animals were hold for 2−3 min, covered the area with fixation tape to ensure that the formulation stays at delivery site, kept on outer surface of the cages for further 5 min before putting them back in the cages. The dose of UMB was selected based on a previous report.[8] The initial paw thickness of the rats was measured by a digital Vernier caliper before starting the treatment. Inflammation was produced in the rat paw by injecting 100 μL of 1%, w/v carrageenan solution in distilled water as an inflammatory agent, into the subplantar region. Paw measurements were taken at stipulated time-points (0.5, 1, 2, 3, and 6 h). The changes in paw thickness over time were recorded for each treatment group, and inflammation (%) was calculated according to the eq (eq 5). The data obtained from the measurements were analyzed to assess the anti-inflammatory effects of the treatments.[43] The changes in paw volume among the nanocomposite gel, conventional gel, and standard groups were compared to that of the control group.

$$\text{Inflammation (\%)} = \frac{(T_t - T_0)}{T_0} \times 100 \quad (5)$$

where T_t = paw thickness after time "t" and T_0 = paw thickness before injection.

2.7.2. Analgesic Study. The analgesic potency of the formulations was evaluated by a rat tail immersion method. Baseline pain sensitivity was determined by measuring the tail withdrawal latency (TWL) of each rat by immersing tail in hot water at 50 °C and the cutoff time was set at 30 s to avoid tissue damage. The rats belonging to the experimental groups received a 400 mg topical application of UMB−MoS_2 nanocomposites (F1), UMB containing gels (F2), diclofenac emulgel (≈2 mg of diclofenac sodium) as standard and negative control (placebo Carbopol 934 gel) to the distal portion of the tail, as per their assigned treatment.[8] The gels were rubbed properly on the site for uniform distribution, and after 5 min, the animals were put back in the clean cages. Each rat underwent repeated TWL measurements at various time points by immersing their tails in the apparatus at predetermined intervals.[44] The TWL measurements were recorded and compared for pain sensitivity between the control and experimental groups.

2.8. Stability Study. The accelerated stability testing was carried out by exposing the UMB−MoS_2 nanocomposite gel (F1) and UMB-containing Carbopol 934 gel (F2) at slightly higher temperature and humidity levels. This study followed the ICH guidelines, wherein the samples were stored at 40 ± 2 °C, along with a relative humidity (RH) of approximately 75 ± 5%, over a period of 6 months. At specific time points (0, 3, and 6 months), samples were withdrawn and subjected to analysis for parameters such as pH, drug content, and spreadability.

2.9. Statistical Data Analysis. The data were presented as the mean with standard deviations, unless otherwise mentioned. The data analysis was done, and plots were generated by GraphPad Prism: V-5.1 (GraphPad Software, Inc., San Diego, CA, USA). A one-way ANOVA followed student's t-test (for in vitro experiments), where p-value less than 0.05 was considered as significant. Bonferroni's multiple comparison test for in vivo analgesic data and best-fit values

https://doi.org/10.1021/acsomega.4c04252
ACS Omega 2024, 9, 37105−37116

after linear regression analysis of the anti-inflammatory data were applied for comparison purpose.

3. RESULTS AND DISCUSSION

3.1. MoS_2 Nanosheet Synthesis and UMB−MoS_2 Nanocomposite Preparation and Its Incorporation into Carbopol 934 Gel. The MoS_2 nanosheets were successfully synthesized by the previously reported one-step hydrothermal reaction method using ammonium-molybdate and thiourea as the reactants.[25] The stepwise synthesis of MoS_2 nanosheets and the formulation of UMB−MoS_2 nanocomposites are shown in Figure 1. The effect of hydrothermal reaction temperatures (such as 180, 200, and 220 °C) and time (such as 6 and 8 h) to get the optimal microstructured thin MoS_2 sheet was investigated well in our previous study by observing the XRD patterns of different synthesized products.[26] The optimal reaction temperature of 220 °C for 8 h of reaction time was found to be the best one to get the microstructured nanosheets of MoS_2. The XRD peaks of the synthesized MoS_2 in the present investigation were found to be in agreement with those of the previous studies.[26,45,46] Therefore, we followed the same reaction conditions to obtain the optimal MoS_2 nanosheets in the present investigation.

The ultrasonic wave-assisted one-step synthesis method was successful to obtain UMB-loaded MoS_2 nanocomposites. A similar approach was exploited in previous studies such as to get a multifunctional MoS_2 nanocomposite for doxorubicin (DOX) delivery and infrared-assisted synergistic photothermal therapy for cancers,[23] MoS_2-graphene oxide (GO) nanocomposites loaded with DOX for targeting and increased anticancer efficacy,[47] MoS_2−MoOx nanocomposites on activated carbon for the electrochemical performance of MoS_2-metal hybrids,[48] and MoS_2-PVP-based nanocomposites for rewritable memory devices with graphene-oxide as electrodes.[49] Taking advantage of this facile synthesis technique, we developed UMB-loaded MoS_2 nanocomposites for the potential topical administration of UMB.

The gel base was prepared beforehand using Carbopol 934, due to its ability to form a gel with a controlled drug release mechanism, even at lower concentrations. The concentration of Carbopol 934 was chosen based on the spreadability and consistency of the gel base. According to previous report,[50] varying concentration of Carbopol 934 (1−4%, w/v) was tried to prepare a drug-loaded gel for topical application, and they found that 2% (w/v) Carbopol 934 was the best one with good consistency, spreadability, homogeneity, etc. Glycerol was used as a humectant in the prepared gels, while triethanolamine at 0.1% (v/v) was used to adjust the pH of the final gel formulations.

3.2. Surface Morphology by Electron Microscopy. The surface morphology of MoS_2 nanosheets can be clearly seen in the SEM image in Figure 2a. The nanosheets are crumpled with each other to form an open-ended structure, as shown in Figure 2a, while the SEM image of the nanocomposite appears to be irregular with a layered structure, as shown in Figure 2b. The nanocomposite has conserved the sheet-like morphology of MoS_2 onto which UMB can be seen being complexed due to its porous nature. However, the structural morphology of the UMB-loaded MoS_2 nanocomposite was also observed under TEM, as shown in Figure 2c. Figure 2c depicts that the nanocomposites were well dispersed in the gel base, indicating the uniform distribution of the nanocarrier in the vehicle.

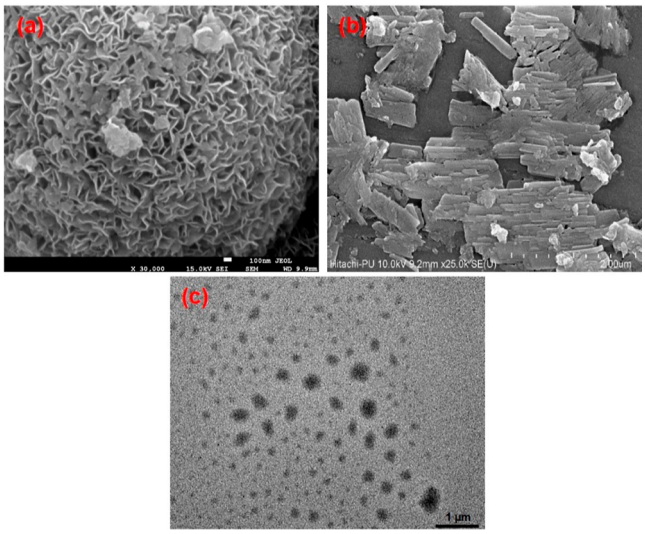

Figure 2. SEM images of UMB−MoS_2 nanosheets (a) and UMB−MoS_2 nanocomposites (b) and the TEM image of UMB−MoS_2 nanocomposites incorporated into Carbopol 934 gel base (c).

3.3. Powder X-ray diffraction. The pXRD diffractograms of the analyzed samples are presented well in Figure 2. The crystal structure analysis of UMB (Figure 3a), MoS_2 (Figure 3b), and UMB-MoS_2 nanocomposite (Figure 3c) as a function of processing parameters was performed by pXRD analysis.

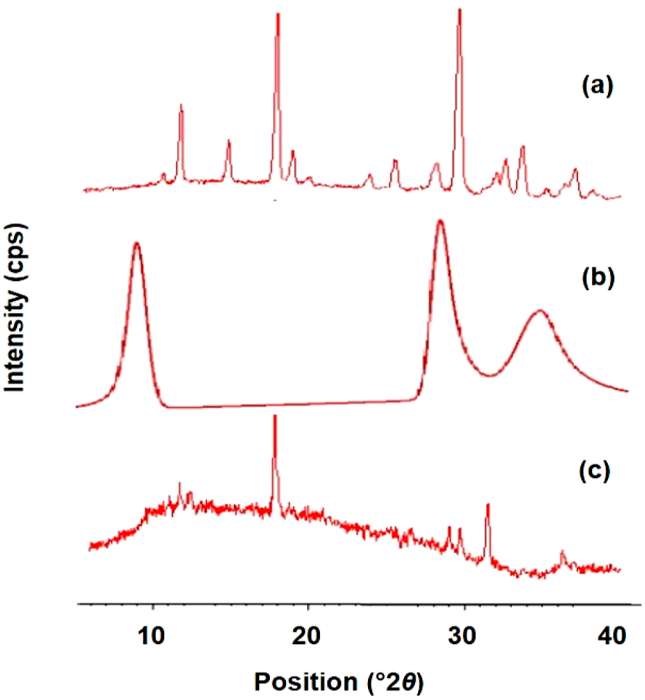

Figure 3. Overlay powdered X-ray diffractograms of pure UMB (a); UMB−MoS_2 (b); and UMB−MoS_2 nanocomposite (c).

The pXRD spectra disclosed the crystalline nature of both UMB due to the presence of sharp and intense peaks (Figure 3a) and MoS_2 with the slightly broadened peaks (Figure 3b) attributed to the fact that as the crystallite size nears the nano range, the pXRD peaks broaden with slightly reduced intensity, respectively. The asymmetric broadened peaks of overlapping and slight shifting toward a lower angle (°2θ) indicate the

https://doi.org/10.1021/acsomega.4c04252
ACS Omega 2024, 9, 37105−37116

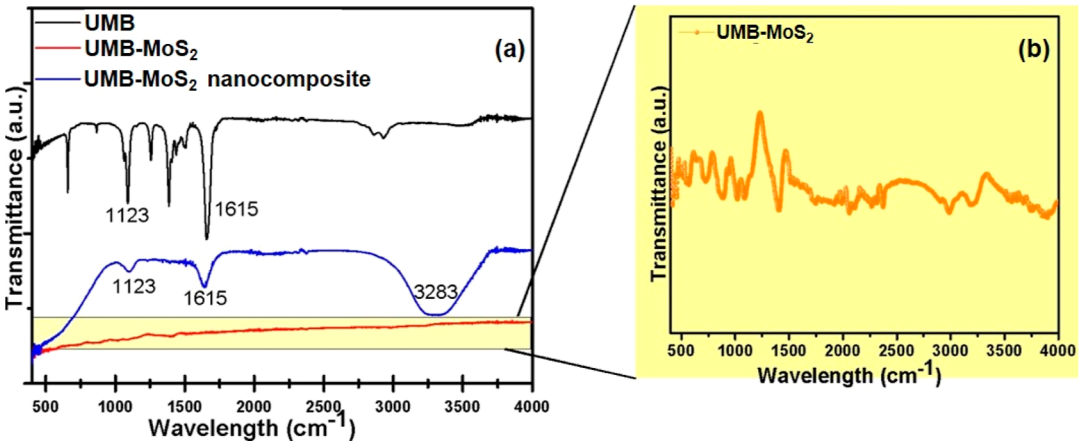

Figure 4. Overlay FTIR spectra of UMB, UMB−MoS_2, and UMB-MoS_2 nanocomposite, all together (a), and the high-resolution FTIR spectrum of UMB−MoS_2 (b).

minimal stacking and shuffling of MoS_2 layers, and the same phenomenon was also observed in previous studies.[51,52] However, the XRD pattern of the UMB−MoS_2 nanocomposite reveals the change of crystalline to amorphous nature when processed in combination showing a molecular interaction (nonbonded) between the drug and the inorganic carrier (MoS_2), as reflected in Figure 3c.

3.4. FTIR Spectroscopy. Figure 4 depicts all the spectra of pure 7-hydroxycoumarin (UMB), molybdenum-disulfide (MoS_2), and the hybrid nanocomposite of both. The FTIR spectrum of UMB (pure) displayed bands at 3177 cm^{-1}, signifying phenolic (−O−H stretching), 1603 cm^{-1} for (C═O stretching), and 1684, 1567 and 1510 cm^{-1} for aromatic (C═C stretching), along with 1319 and 1135 cm^{-1} for (C−O−C stretching). Similar typical IR spectrum bands of UMB were also seen during the evaluation of anti-inflammatory potential of UMB when the UMB film was complexed with the matrix of phospholipids.[8] In contrast, the FTIR spectrum of MoS_2 exhibited two vibrational modes around 3185 cm^{-1}, which are attributed to hydroxyl functionalities derived from moisture adsorption on MoS_2 from the atmosphere. Additionally, broad absorption bands at 556, 639, 889.39, and 1402.99 cm^{-1} were associated with MoS_2, which were also observed during the photocatalytic activity evaluation of MoS_2 nanoparticles[53] and photothermal cancer therapeutic potential of PEG-coated MoS_2 nanoflakes.[54] The presence of S−S bonds was indicated by the peak at 483 cm^{-1}, and another S−S bond was suggested by the 938 cm^{-1} peak. Peaks at approximately 3200 cm^{-1} were indicative of the characteristic bands of the O−H group's characteristic bands. Conclusively, in the case of their hybrid nanocomposite, the FTIR spectra clearly show that the peaks have been shifted at 1100 and 1638 cm^{-1}, which confirms the formation of the complex. Also, the 3283 cm^{-1} peak corresponds to the characteristic bands of the O−H group's characteristic bands. Thus, the results show the successful incorporation of UMB in MoS_2.

3.5. Particle Size and Polydispersity-Index. The UMB−MoS_2 hybrid nanocomposite has shown an average particle size of 435.1 ± 22.8 nm, as shown in Figure 5. The obtained size of the nanocomposite was found to be within the limit for an efficient topical application. According to the available literature, the polymeric NPs with a size range up to 700 nm can gather in and around the hair follicles and serve as a depot system for prolonged drug diffusion across the cells.[55]

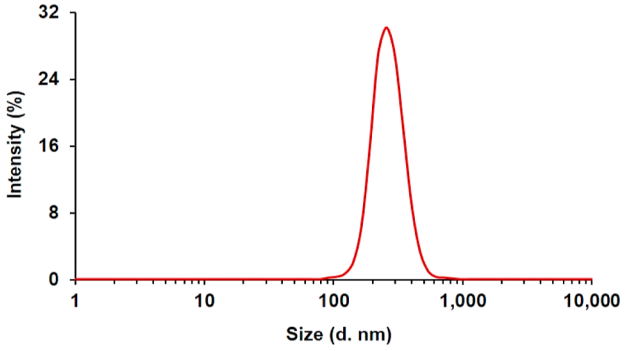

Figure 5. Particle size distribution of the optimal UMB−MoS_2 hybrid nanocomposites.

Therefore, we considered that the obtained size of the nanocomposites was smaller, which would facilitate the permeation across the skin while applied topically as reported in previous literature.[56,57] However, the PDI was 0.415 ± 0.105, which signifies that the particle size distribution was unimodal and moderate within the range.

3.6. Percentage Yield. The percentage yield of the UMB−MoS_2 nanocomposite was found to be 96.2 ± 3.4%. The greater yield values indicate that the loss of raw materials was low, which signifies that the formulation process was optimal and significant. The yield of nanocomposites in the present study was comparable and in agreement with previous studies which followed the same hydrothermal method to prepare the MoS_2 nanosheets for multiple purposes including pharmaceutical and pollution reduction[58] as well as water remediation and energy storage applications.[59−61]

3.7. pH, Spreadability, and Viscosity of UMB-MoS_2 Nanocomposite Gel (F1) and Conventional Gel (F2) and Drug Content Determination. The deviation from the recommended pH may lead to skin irritation or other unwanted side effects. The pH values of F1 and F2 were found to be 5.56 ± 0.12 and 5.62 ± 0.18, respectively, which are well within the range for topical delivery. Both formulations F1 and F2 showed spreadability values of 5.89 ± 0.42 and 6.72 ± 0.19 g·cm/s, respectively, which were suitable for topical application. These values suggested that the prepared gel had good spreadability and adhesiveness even after applying a small magnitude of shear, which were also reported for nano-formulations for dermal applications.[56,62,63] The viscosities of

https://doi.org/10.1021/acsomega.4c04252
ACS Omega 2024, 9, 37105−37116

F1 and F2 at 10−250 s^{-1} shear rate and 25 °C were 32.5 ± 1.9 and 28.7 ± 2.1 Pa s, which were optimal for topical application,[64] as highly viscous gels may have poor spreadability and too low viscous spread fast and runs off quickly from the applied surfaces. It is an important characteristic of topically applied gel-based products. It influences the drug release rate, skin application (skin-feel and spreadability), and permeation. The viscosity of the gels (F1 and F2) decreased exponentially as the shear rate increased, i.e., it first decreased sharply which later became gradual revealing the shear thinning nature of the gel, as shown in Figure 6. The viscosity

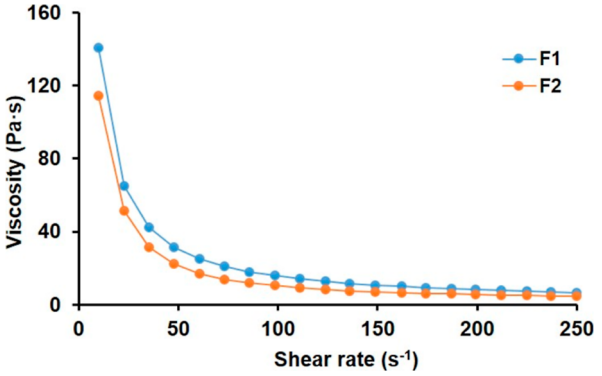

Figure 6. Viscosity versus shear rate plot of both the gel-based formulations (Carbopol 934 gel, i.e., F1, and UMB−MoS_2 nanocomposite gel, i.e., F2). Both the gels exhibited a decreasing viscosity with increasing shear rate (shear thinning behavior).

graph of both the formulations exhibits a decreasing trend with increasing shear rate (shear thinning phenomenon), which was a desirable property for topical formulations as it facilitates application through rubbing, which reduces viscosity, enabling even distribution.

It suggests that the gel was well-suited for topical delivery as it can be applied easily and provides good coverage. However, at rest, the polymer chains are tangled up, which prevents flow, allowing the thick gel to stay in place. The drug contents of F1 and F2 were found to be 68.4 ± 1 and 94.1 ± 1.2%, respectively, which indicated the sufficient incorporation of pure-UMB and UMB−MoS_2 nanocomposites into the Carbopol 934 gel base in the case of F2 and F1. A comparatively lower drug content in the case of UMB−MoS_2 nanocomposite (F1) was obtained, which might be due to the proper incorporation and complexation of UMB with MoS_2, which lead to a slower release of UMB from the nanocomposite gel which in turn resulted in lower concentration of free drug.

3.8. In Vitro Drug Release Assessment. The comparative drug release analysis was performed using the dialysis bag method, and the release profiles are shown in Figure 7. The UMB−MoS_2 nanocomposite-loaded Carbopol 934 gel (F1) has shown a biphasic drug release pattern, as the release of drug was quick initially (up to 3 h, around 65.7 ± 3.6%) and thereafter became slow and gradual in later stages. The initial higher and faster drug release is due to the presence of free or loosely incorporated drug molecules on the surface or within the porous structure of the nanocomposite. Apart from this, the increased drug release from F1 was due to the amorphous conversion of UMB from its crystalline state. The amorphous form of poorly aqueous soluble drug(s) has obviously higher aqueous solubility and release as compared to its crystalline

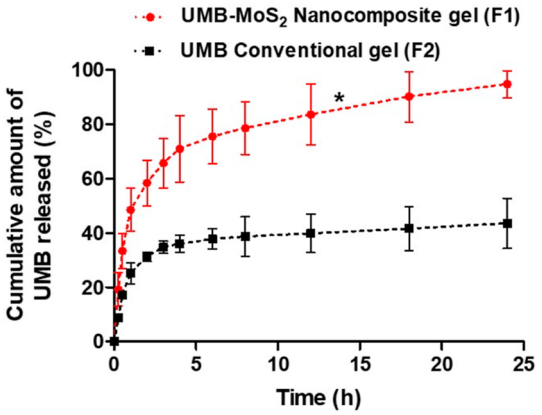

Figure 7. In vitro drug release profile of the UMB−MoS_2 nanocomposite containing gel (F1) and conventional Carbopol 934-based gel containing UMB (F2). "Data are the average of three measurements with standard deviation (mean ± SD, n = 3), where * represents $p < 0.005$ as compared to the UMB conventional gel (F2)".

state and thus improve its biopharmaceutical properties. In the case of transdermal application, the amorphous of drug molecules dispersed in gel base drug delivery carriers have shown marked improvement in skin penetration.[65] However, subsequent release was slowed down, which might be due to adsorption and complexation of drug molecules in MoS_2. This interaction acts as a drug reservoir, hindering the diffusion of the drug molecules into the surrounding environment. Consequently, a more sustained release profile is achieved, with up to 94.8 ± 4.7% released over a period of 24 h. In the case of conventional gel (F2), the release pattern of UMB was similar to that of F1 up to 3 h, which was 34.7 ± 1.9%, but the release was comparatively less at all-time points. Nevertheless, it became stagnant in the later stages of the study and could release only 43.5 ± 3.7% at 24 h. The pure UMB gel exhibited slow and incomplete drug release throughout due to the limited solubility of UMB in the aqueous gel base, restricting the available drug for dissolution, compounded by its lower surface area compared to the nanocomposite gel, limiting the release area. Moreover, the better release profile of the UMB−MoS_2 nanocomposite from the gel base is due to a number of contributing factors such as the high surface area to volume ratio of the nanosized formulation and the conversion of the crystalline nature of MoS_2 to relatively amorphous nature of the UMB−MoS_2 nanocomposite, leading to an improvement in the drug dissolution and sustained drug release as a result of composite formation.

The result of release modeling is summarized in Table 1, which represented the calculated values of coefficient of determination (R^2), rate constants (k) of different models, and the diffusion-exponent (n-value) of the best-fit models. The formulation (F1) followed the first-order release model as the R^2 value was the highest (0.94) for this model, which describes the drug release from a polymeric system. However, F2 followed the Higuchi-matrix model as the R^2 was 0.83 (highest among the applied models). Additionally, the mechanism of drug release from both the gel formulations can be categorized to Fickian-diffusion as the n-values were 0.019 and 0.0.129 for F1 and F2, respectively, which falls between 0 and 0.5, i.e., < 0.5. Application release modeling suggested that the release of UMB from F1 and F2 followed a mechanism that was

https://doi.org/10.1021/acsomega.4c04252
ACS Omega 2024, 9, 37105−37116

Table 1. Drug Release Kinetics Modeling of UMB−MoS_2 Nanocomposite Gel (F1) and Conventional Carbopol 934-Based Gel Containing Free UMB (F2)[a]

formulations	zero order		first order			Higuchi model			Korsmeyer−Peppas model		Hixon−Crowell	
	R^2	k_0	R^2	k_1	"n"	R^2	k_{HM}	"n"	R^2	k_{KP}	R^2	K_{HC}
nanocomposite gel (F1)	0.66	0.29	0.94	3.51	0.019	0.84	0.35		0.90	0.59	0.86	13.8
conventional gel (F2)	0.52	0.14	0.58	3.75		0.83	0.18	0.129	0.56	0.29	0.73	13.7

[a] R^2 = coefficient of determination; k_0 = zero-order; k_1 = first-order; kHM = Higuchi-matrix model; kKP = Korsmeyer−Peppas model; and KHC = Hixon−Crowell rate constants, whereas "n" = release/diffusion exponent values.

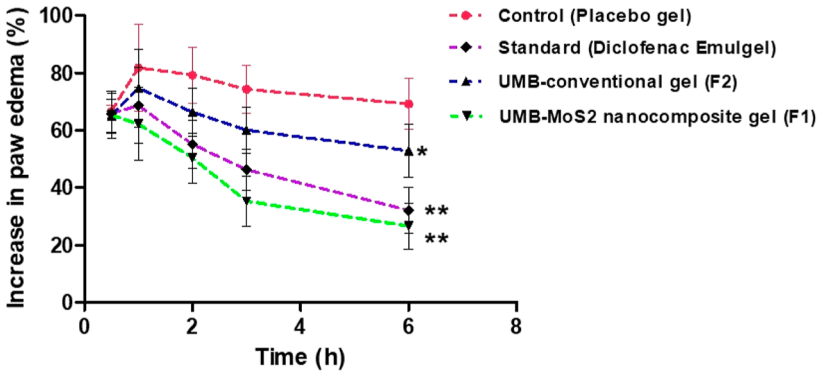

Figure 8. Comparative anti-inflammatory effect exerted by control (placebo Carbopol 934 gel), UMB−MoS_2 nanocomposite gel (F1), UMB containing conventional gel (F2), and standard formulation (diclofenac emulgel) in a carrageenan-induced rat paw edema model. Data were represented as mean with standard deviation (mean ± SD, n = 6), where * represents a significant difference (p < 0.05) between F2 (UMB−conventional gel) and the control group (placebo gel), ** represents an equivalent effect by standard treatments (diclofenac emulgel and F1 treatments), and both exerted significant (p < 0.05) effect as compared to other two groups (control and F2 groups).

anomalous and controlled by a combination of diffusion and swelling and erosion of polymeric-matrix.

In the case of the first-order kinetic model as observed for F1, the rate constant is directly linked to the initial drug and nature of polymer (in case of the polymeric drug delivery system), which was also discussed for the release of acyclovir from MgO-nanocomposite incorporated in acrylamide-based hydrogel.[66] The first-order release kinetics partly redirect the reservoir-type delivery system. The flexibility of the polymer chains of Carbopol 934 further delayed the drug release due to dense cross-linking in the network of the polymer. The Higuchi model (as observed for F2) demonstrates that the drug release was controlled by the diffusion-mechanism of drug release, which was also demonstrated when the graphene−chitosan-based nanocomposite was used for the release of anticancer drugs.[67] Under similar pH conditions, the release of UMB from F2 was low where the drug was incorporated into the Carbopol 934 gel base. This might be due to the fact that when gels come in contact with the release medium, the hydrophilic gel itself served as releasing channels for interior (in the polymer-network) drug molecules. Thus, the interphase between the polymer network and release medium could control and slow down the release of UMB from F2.

3.9. Bioadhesive Strength. Both the nanocomposite gel (F1) and the conventional gel (F2) exhibited bioadhesive strengths within the optimal range for topical application, measuring 0.09 ± 0.01 and 0.08 ± 0.01 N/cm2, respectively. This moderate bioadhesive property facilitates the formulations' adherence to the site of administration, enabling prolonged drug permeation. Carbopol gel base adheres to the skin through a two-pronged approach. First, its high viscosity and hydrophilicity enable close contact with the skin's surface, allowing it to hydrate and swell. Then, the acrylic polymer chains in Carbopol form hydrogen bonds with the polar groups in skin's keratin contributing to the bioadhesive nature of formulation.[68,69] Importantly, the bioadhesive strength is not excessively high, which could otherwise lead to difficulties in removal and residual greasiness after application.

3.10. In Vivo Anti-inflammatory Activity. The anti-inflammatory activity of control (placebo Carbopol 934 gel), UMB-MoS_2 nanocomposite gel (F1), UMB containing conventional gel (F2), and standard formulation (diclofenac emulgel) was examined by the carrageenan-induced rat paw edema model. The comparative anti-inflammatory activity profiles of all of the groups are shown in Figure 8.

Carrageenan produced pronounced edema, which peaked after 1 h of administration. The control group had the least improvement and had marked edema at around 69.2 ± 3.6% after 6 h. Initially, UMB containing a conventional Carbopol 934 gel (F2) controlled the paw edema better than the control but less than the UMB−MoS_2 nanocomposite gel (F1), but the effect became steadier toward the end and could only reduce the edema to 52.9 ± 3.7%. The nanocomposite loaded gel (F1) was able to ameliorate the paw edema with a similar pattern as that obtained with standard (diclofenac emulgel) treatment. Both these formulations have shown greater potential than that of other treatments (F2 as well as control) at all-time points as the nanocomposite (F1) and diclofenac emulgel restricted the edema to 26.6 ± 3.2 and 32.2 ± 3.2%, respectively. The results of rat paw edema treatment by a UMB-containing formulation show significantly reduced edema with improved antinociceptive effects, which was also found when anti-inflammatory and analgesic activities of *Justicia pectoralis* (contains UMB) were evaluated.[12,70,71] Similarly, anti-inflammatory activity and edema inhibition

https://doi.org/10.1021/acsomega.4c04252
ACS Omega 2024, 9, 37105−37116

were noted in the case of the UMB-matrix film loaded phospholipid complex in carrageenan-induced paw edema in rats.[8] Thus, the results of our study have shown that the UMB−MoS_2 nanocomposite gel (F1) provided the significant inhibition in the paw edema, which was in agreement with the earlier reports.[8,72] The improved anti-inflammatory activity of F1 advocates for the additive effect of MoS_2 acting as an anti-inflammatory agent itself in addition to the role of nanocarriers along with UMB.

3.11. In Vivo Analgesic Activity. The analgesic potential of the UMB-formulations was assessed using the tail immersion method, where the latency in tail withdrawal response by the rat was measured as a parameter for evaluating analgesic activity.

Based on analgesic activity results, it was indicated that the control group exhibited minimal changes in TWL ranging between 5.5 ± 0.5 and 5.9 ± 1.2 s. The TWL of the conventional gel (F2) increased initially from 5.9 ± 0.7 s to the peak of 6.9 ± 0.8 s half an hour of post application before declining and, afterward, to 5.6 ± 0.9 s at the end of the experiment. The UMB-MoS_2 nanocomposite gel (F1) exhibited analgesic activity superior to all other treated groups, as depicted in Figure 9. The TWL of the F1-treated group progressively increased from 6.6 ± 1.4 s until reaching its peak after 2 h at 10.9 ± 2.1 s, followed by a slight decrease to 10.2 ± 1.8 s, whereas the standard group had the TWL in the range of 6.1 ± 1.1 to 10 ± 2 s. The decreased pain sensitivity seen in the group treated with the UMB nanocomposite gel showed that formulating UMB as a nanocomposite greatly enhanced its analgesic properties. Specifically, the UMB−MoS_2 nanocomposite gel (F1) exhibited superior pain relief as compared to the standard preparation (diclofenac emulgel), whereas the UMB-containing conventional gel (F2) was not able to match with F1 and the standard preparation. The potential analgesic activity of UMB-containing formulations in this study is in agreement with the previous reports.[70,71] A detailed statistical analysis performed by one-way ANOVA followed by Bonferroni's multiple comparison test by GraphPad Prism for comparative analgesic activity is mentioned in Table S1 (Supporting Information), and best-fit values after linear regression analysis of the anti-inflammatory data are summarized in Table S2 (Supporting Information). Similarly, improved pain relieving effects of UMB formulations in the carrageenan-based rat model were noted in previous reports, where they proved that the antinociceptive effect of UMB was through the nitric-oxide system rather than opioid-based system by inhibiting the centrally as well as peripherally acting chemical pain mediators.[12,70,71]

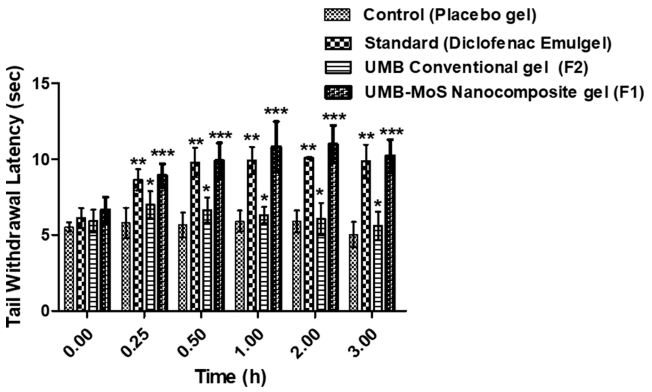

Figure 9. Comparative analgesic effect of control (Carbopol 934 gel without UMB), UMB−MoS_2 nanocomposite gel, conventional gel (pure-UMB in Carbopol 934 gel base), and standard diclofenac emulgel by the tail emersion method. "Data were represented as mean with standard deviation (mean ± SD, n = 6), where * represents a significant difference (p < 0.05) between the conventional gel (F2) and the control group, ** represents a significant difference (p < 0.05) between the diclofenac emulgel and other two groups (control and F2 groups), while *** represents a significant difference (p < 0.05) between F1 and other treated groups".

3.12. Stability Study. Neither the UMB−MoS_2 containing nanocomposite gel (F1) nor the conventional gel containing pure UMB showed any significant changes during the storage for 6 months under the stressed conditions (40 ± 2 °C with 75 ± 5% RH). In the mentioned storage conditions, the samples were analyzed for different parameters, and results are well summarized in Table 2. The obtained results indicate that both the UMB-containing formulations (F1 and F2) were found to be stable at 40 ± 2 °C with 75 ± 5% RH for 6 months of storage.

4. CONCLUSIONS

In this study, MoS_2 nanosheets were successfully synthesized via a green hydrothermal method and complexed with UMB using an ultrasonic-assisted technique to form an organic−inorganic UMB−MoS_2 nanocomposite. Characterization studies confirmed the nanocomposite formation with a size of 435 nm and 0.415 PDI, suitable for topical application. FTIR spectra revealed modified functional groups due to the UMB−MoS_2 interaction, while pXRD and SEM analyses indicated an amorphous nature and porous structure of the nanocomposite, respectively, suggesting improved solubility. The UMB−MoS_2 nanocomposite was incorporated into a Carbopol 934 gel base (F1), exhibiting optimal pH (5.56), spreadability (5.89 g·cm/s), and viscosity (32.5 Pa s), suitable for topical use. Notably, F1 demonstrated a biphasic and significantly higher drug release (94.8%) as compared to the pure-UMB gel (F2, 43.5%) in 24 h, following first-order kinetics with a Fickian diffusion mechanism. In vivo studies revealed that F1 effectively inhibited edema formation (26.6%) compared to the standard treatment (32.16%), indicating superior anti-inflammatory

Table 2. Stability Profile of the UMB−MoS_2 Nanocomposite Gel (F1) and UMB-Containing Conventional Carbopol 934-Based Gel (F2) at Different Time Points Stored at 40 ± 2 °C and 75 ± 5% RH[a]

time	pH		spreadability (cm g/s)		drug content (%)	
	F1	F2	F1	F2	F1	F2
initially (0 h)	5.56 ± 0.12	5.62 ± 0.18	5.89 ± 0.42	6.72 ± 0.19	68.4 ± 1.1	98.1 ± 1.2
At 3 months	5.55 ± 0.19	5.65 ± 0.25	5.81 ± 0.51	6.64 ± 0.42	67.2 ± 2.1	97.7 ± 1.8
At 6 months	5.58 ± 0.22	5.68 ± 0.21	5.77 ± 0.68	6.62 ± 0.28	67.4 ± 1.6	97.5 ± 2.0

[a]The data were presented as an average of three measurements with standard deviations (mean ± SD, n = 3).

https://doi.org/10.1021/acsomega.4c04252
ACS Omega 2024, 9, 37105−37116

activity with enhanced analgesic effects by prolonging the TWL. These improved therapeutic performances were also attributed to the increased UMB release from F1 a potential synergistic effect of UMB and MoS_2. Overall, the MoS_2-based nanocomposite gel system improved the in vitro and in vivo performances of UMB, showing its promising biomedical application potential. Further in vivo pharmacokinetic and pharmacodynamic studies are warranted to elucidate the potential of the UMB-MoS_2 nanocomposite gel and the synergistic mechanism between the UMB and inorganic MoS_2.

■ ASSOCIATED CONTENT

Data Availability Statement

"Data used are available throughout the manuscript text".

Supporting Information

The Supporting Information is available free of charge at https://pubs.acs.org/doi/10.1021/acsomega.4c04252.

One-way ANOVA test results and best-fit values after linear regression analysis of the anti-inflammatory data (PDF)

■ AUTHOR INFORMATION

Corresponding Author

Bhavna Kumar − *Faculty of Pharmacy, DIT University, Dehradun 248009 Uttarakhand, India;* orcid.org/0000-0001-7429-8047; Email: bhavna@dituniversity.edu.in

Authors

Diwya Kumar Lal − *Faculty of Pharmacy, DIT University, Dehradun 248009 Uttarakhand, India*

Vishakha Kaushik − *School of Physical Sciences, DIT University, Dehradun 248009 Uttarakhand, India*

Adel Alhowyan − *Department of Pharmaceutics, College of Pharmacy, King Saud University, Riyadh 11451, Saudi Arabia*

Mohd Abul Kalam − *Department of Pharmaceutics, College of Pharmacy, King Saud University, Riyadh 11451, Saudi Arabia;* orcid.org/0000-0002-5713-8858

Complete contact information is available at: https://pubs.acs.org/10.1021/acsomega.4c04252

Funding

"This work was funded by the Researchers Supporting Project number (RSPD2024R726), King Saud University, Riyadh, Saudi Arabia".

Notes

The authors declare no competing financial interest.

■ ACKNOWLEDGMENTS

The authors extend their appreciation to the Researchers Supporting Project number (RSPD2024R726), King Saud University, Riyadh, Saudi Arabia. We are also thankful to the Center for Excellence MNRL, DIT University, and Dr. Gopal from the School of Petroleum, DIT University, Dehradun, for providing technical support and resources for this research work.

■ REFERENCES

(1) Ansar, W.; Ghosh, S. Inflammation and inflammatory diseases, markers, and mediators: Role of CRP in some inflammatory diseases. In *Biology of C reactive protein in health and disease*; Springer India, 2016; pp 67−107.

(2) Maurya, A. K.; Mohanty, S.; Pal, A.; Chanotiya, C. S.; Bawankule, D. U. The essential oil from Citrus limetta Risso peels alleviates skin inflammation: In-vitro and in-vivo study. *J. Ethnopharmacol.* **2018**, *212*, 86−94.

(3) Eyerich, K.; Eyerich, S. Immune response patterns in non-communicable inflammatory skin diseases. *J. Eur. Acad. Dermatol Venereol* **2018**, *32* (5), 692−703.

(4) Zeng, W. J.; Tan, Z.; Lai, X. F.; Xu, Y. N.; Mai, C. L.; Zhang, J.; Lin, Z. J.; Liu, X. G.; Sun, S. L.; Zhou, L. J. Topical delivery of l-theanine ameliorates TPA-induced acute skin inflammation via downregulating endothelial PECAM-1 and neutrophil infiltration and activation. *Chem.-Biol. Interact.* **2018**, *284*, 69−79.

(5) Sawada, Y.; Saito-Sasaki, N.; Mashima, E.; Nakamura, M. Daily Lifestyle and Inflammatory Skin Diseases. *Int. J. Mol. Sci.* **2021**, *22*, 5204.

(6) Sohail, R.; Mathew, M.; Patel, K. K.; Reddy, S. A.; Haider, Z.; Naria, M.; Habib, A.; Abdin, Z. U.; Razzaq Chaudhry, W.; Akbar, A. Effects of Non-steroidal Anti-inflammatory Drugs (NSAIDs) and Gastroprotective NSAIDs on the Gastrointestinal Tract: A Narrative Review. *Cureus* **2023**, *15* (4), No. e37080.

(7) Vasconcelos, J. F.; Teixeira, M. M.; Barbosa-Filho, J. M.; Agra, M. F.; Nunes, X. P.; Giulietti, A. M.; Ribeiro-dos-Santos, R.; Soares, M. B. P. Effects of umbelliferone in a murine model of allergic airway inflammation. *Eur. J. Pharmacol.* **2009**, *609* (1−3), 126−131.

(8) Telange, D. R.; Nirgulkar, S. B.; Umekar, M. J.; Patil, A. T.; Pethe, A. M.; Bali, N. R. Enhanced transdermal permeation and anti-inflammatory potential of phospholipids complex-loaded matrix film of umbelliferone: Formulation development, physico-chemical and functional characterization. *Eur. J. Pharm. Sci.* **2019**, *131*, 23−38.

(9) Muthu, R.; Selvaraj, N.; Vaiyapuri, M. Anti-inflammatory and proapoptotic effects of umbelliferone in colon carcinogenesis. *Hum. Exp. Toxicol.* **2016**, *35* (10), 1041−1054.

(10) Wu, G.; Nie, W.; Wang, Q.; Hao, Y.; Gong, S.; Zheng, Y.; Lv, H. Umbelliferone Ameliorates Complete Freund Adjuvant−Induced Arthritis via Reduction of NF-κB Signaling Pathway in Osteoclast Differentiation. *Inflammation* **2021**, *44* (4), 1315−1329.

(11) Lim, J.-y.; Lee, J.-H.; Lee, D.-H.; Lee, J.-H.; Kim, D.-K. Umbelliferone reduces the expression of inflammatory chemokines in HaCaT cells and DNCB/DFE-induced atopic dermatitis symptoms in mice. *Int. Immunopharmacol.* **2019**, *75*, 105830.

(12) Rauf, A.; Khan, R.; Khan, H.; Pervez, S.; Pirzada, A. S. In vivo antinociceptive and anti-inflammatory activities of umbelliferone isolated from Potentilla evestita. *Nat. Prod. Res.* **2014**, *28* (17), 1371−1374.

(13) Singh, R.; Singh, B.; Singh, S.; Kumar, N.; Kumar, S.; Arora, S. Umbelliferone − An antioxidant isolated from Acacia nilotica (L.) Willd. Ex. Del. *Food Chem.* **2010**, *120* (3), 825−830.

(14) Abeesh, P.; Guruvayoorappan, C. Umbelliferone loaded PEGylated liposomes: preparation, characterization and its mitigatory effects on Dalton's ascites lymphoma development. *3 Biotech* **2023**, *13* (6), 216.

(15) Sun, G.; Yang, S.; Cai, H.; Shu, Y.; Han, Q.; Wang, B.; Li, Z.; Zhou, L.; Gao, Q.; Yin, Z. Molybdenum disulfide nanoflowers mediated anti-inflammation macrophage modulation for spinal cord injury treatment. *J. Colloid Interface Sci.* **2019**, *549*, 50−62.

(16) Chhowalla, M.; Shin, H. S.; Eda, G.; Li, L.-J.; Loh, K. P.; Zhang, H. The chemistry of two-dimensional layered transition metal dichalcogenide nanosheets. *Nat. Chem.* **2013**, *5* (4), 263−275.

(17) Lcc, A. M. *Safety Data Sheet − Molybdenum Disulfide (MoS_2)*, 2020. https://www.acsmaterial.com/pub/media/catalog/product/file/SDS-Molybdenum_Disulfide_MoS2_.pdf (accessed 2020 01 02).

(18) Chen, W.; Qi, W.; Lu, W.; Chaudhury, N. R.; Yuan, J.; Qin, L.; Lou, J. Direct Assessment of the Toxicity of Molybdenum Disulfide Atomically Thin Film and Microparticles via Cytotoxicity and Patch Testing. *Small* **2018**, *14* (12), No. e1702600.

(19) Teo, W. Z.; Chng, E. L. K.; Sofer, Z.; Pumera, M. Cytotoxicity of Exfoliated Transition-Metal Dichalcogenides (MoS2, WS2, and WSe2) is Lower Than That of Graphene and its Analogues. *Chem. - Eur. J.* **2014**, *20* (31), 9627−9632.

(20) Li, B. L.; Setyawati, M. I.; Chen, L.; Xie, J.; Ariga, K.; Lim, C.-T.; Garaj, S.; Leong, D. T. Directing Assembly and Disassembly of 2D MoS2 Nanosheets with DNA for Drug Delivery. *ACS Appl. Mater. Interfaces* **2017**, *9* (18), 15286−15296.
(21) Zhang, X.; Wu, J.; Williams, G. R.; Niu, S.; Qian, Q.; Zhu, L.-M. Functionalized MoS2-nanosheets for targeted drug delivery and chemo-photothermal therapy. *Colloids Surf., B* **2019**, *173*, 101−108.
(22) Zhang, A.; Li, A.; Tian, W.; Li, Z.; Wei, C.; Sun, Y.; Zhao, W.; Liu, M.; Liu, J. A Target-Directed Chemo-Photothermal System Based on Transferrin and Copolymer-Modified MoS2 Nanoplates with pH-Activated Drug Release. *Chem.—Eur. J.* **2017**, *23* (47), 11346−11356.
(23) Liu, J.; Lu, K.; Gao, F.; Zhao, L.; Li, H.; Jiang, Y. Multifunctional MoS2 composite nanomaterials for drug delivery and synergistic photothermal therapy in cancer treatment. *Ceram. Int.* **2022**, *48* (15), 22378−22386.
(24) Qiu, W.; Zhao, W.; Zhang, L.; Wang, H.; Li, N.; Chen, K.; Zhang, H.; Wang, Y. A Solid−Liquid Composite Lubricating "Nano-Snowboard" for Long-Acting Treatment of Osteoarthritis. *Adv. Funct. Mater.* **2022**, *32* (46), 2208189.
(25) Duraisamy, S.; Ganguly, A.; Sharma, P. K.; Benson, J.; Davis, J.; Papakonstantinou, P. One-Step Hydrothermal Synthesis of Phase-Engineered MoS2/MoO3 Electrocatalysts for Hydrogen Evolution Reaction. *ACS Appl. Nano Mater.* **2021**, *4* (3), 2642−2656.
(26) Kaushik, V.; Kumari, N.; Bhojani, A. K.; Singh, D. K.; Pathak, S. Rheological and shear thickening properties in MoS2 nanosheets dispersion: An integrated experimental and theoretical investigation. *Phys. B* **2024**, *673*, 415453.
(27) Rahman, M.; Singh, J. G.; Afzal, O.; Altamimi, A. S. A.; Alrobaian, M.; Haneef, J.; Barkat, M. A.; Almalki, W. H.; Handa, M.; Shukla, R.; et al. Preparation, Characterization, and Evaluation of Curcumin−Graphene Oxide Complex-Loaded Liposomes against Staphylococcus aureus in Topical Disease. *ACS Omega* **2022**, *7* (48), 43499−43509.
(28) Sadhanala, H.; Senapati, S.; Harika, K. V.; Nanda, K. K.; Gedanken, A. Green synthesis of MoS 2 nanoflowers for efficient degradation of methylene blue and crystal violet dyes under natural sun light conditions. *New J. Chem.* **2018**, *42* (17), 14318−14324.
(29) Gan, Y. X. Structural assessment of nanocomposites. *Micron* **2012**, *43* (7), 782−817.
(30) Ragab, H. M. Studies on the thermal and electrical properties of polyethylene oxide/polyvinyl alcohol blend by incorporating of Cesium Chloride. *Results Phys.* **2017**, *7*, 2057−2065.
(31) Kalam, M. A.; Ali, R.; Alhowyan, A.; Ahmad, A.; Iqbal, M.; Raish, M. J. J. o. D. D. S. Quercetin-loaded transliposomal gel for effective management of skin cancer: In vitro and cell line efficacy studies. *J. Drug Delivery Sci. Technol.* **2024**, *96*, 105659.
(32) Ganguly, M.; Pramanik, D. Pectin coated iron oxide nanocomposite-a vehicle for controlled release of curcumin. *Int. J. Biol. Biomed Eng.* **2017**, *11*, 143−160.
(33) Chin, I. b. I.; Yenn, T. W.; Ring, L. C.; Lazim, Y.; Tan, W.-N.; Rashid, S. A.; Yuan, C. S.; Yet, Z. R.; Abdullah, S. Z.; Taher, M. A. Phomopsidione-Loaded Chitosan Polyethylene Glycol (PEG) Nanocomposite Dressing for Pressure Ulcers. *J. Pharm. Sci.* **2020**, *109* (9), 2884−2890.
(34) Sadeghi-Ghadi, Z.; Behjou, N.; Ebrahimnejad, P.; Mahkam, M.; Goli, H. R.; Lam, M.; Nokhodchi, A. c. *J. Pharm. Innovation* **2023**, *18* (1), 13−28.
(35) Lukić, M.; Pantelić, I.; Savić, S. D. Towards optimal ph of the skin and topical formulations: From the current state of the art to tailored products. *Cosmetics* **2021**, *8* (3), 69.
(36) Saab, M.; Raafat, K.; El-Maradny, H. Transdermal Delivery of Capsaicin Nanoemulgel: Optimization, Skin Permeation and In Vivo Activity against Diabetic Neuropathy. *Adv. Pharm. Bull.* **2022**, *12* (4), 780−790.
(37) Ge, J.; Wu, Q.; Ding, L.; Guo, H.; Zhao, A. Preparation and rheological Evaluation of a thixotropic polymer gel for water shutoff in fractured tight reservoirs. *J. Pet. Sci. Eng.* **2022**, *208*, 109542.
(38) Kumar, M.; Shanthi, N.; Mahato, A. K.; Soni, S.; Rajnikanth, P. S. Preparation of luliconazole nanocrystals loaded hydrogel for improvement of dissolution and antifungal activity. *Heliyon* **2019**, *5* (5), No. e01688.
(39) Malik, A.; Kushnoor, A.; Saini, V.; Singhal, S.; Kumar, S.; Chand Yadav, Y. Analytical method development of nutraceutical: Umbelliferone. *Pharma Sci. Monit.* **2012**, *3* (1), 67.
(40) Ahmed, M. M.; Fatima, F.; Anwer, M. K.; Ibnouf, E. O.; Kalam, M. A.; Alshamsan, A.; Aldawsari, M. F.; Alalaiwe, A.; Ansari, M. J. Formulation and in vitro evaluation of topical nanosponge-based gel containing butenafine for the treatment of fungal skin infection. *Saudi Pharm. J.* **2021**, *29* (5), 467−477.
(41) Permana, A. D.; Utami, R. N.; Layadi, P.; Himawan, A.; Juniarti, N.; Anjani, Q. K.; Utomo, E.; Mardikasari, S. A.; Arjuna, A.; Donnelly, R. F. Thermosensitive and mucoadhesive in situ ocular gel for effective local delivery and antifungal activity of itraconazole nanocrystal in the treatment of fungal keratitis. *Int. J. Pharm.* **2021**, *602*, 120623.
(42) Ullah, N.; Amin, A.; Farid, A.; Selim, S.; Rashid, S. A.; Aziz, M. I.; Kamran, S. H.; Khan, M. A.; Rahim Khan, N.; Mashal, S.; et al. Development and Evaluation of Essential Oil-Based Nanoemulgel Formulation for the Treatment of Oral Bacterial Infections. *Gels* **2023**, *9* (3), 252.
(43) Raut, S. Y.; Gahane, A.; Joshi, M. B.; Kalthur, G.; Mutalik, S. Nanocomposite clay-polymer microbeads for oral controlled drug delivery: Development and, in vitro and in vivo evaluations. *J. Drug Delivery Sci. Technol.* **2019**, *51*, 234−243.
(44) Ullah, Q.; Ali, Z.; Rashid, U.; Ali, G.; Ahmad, N.; Khan, R.; Ullah, S.; Ayaz, M.; Murthy, H. C. A. Involvement of the Opioidergic Mechanism in the Analgesic Potential of a Novel Indazolone Derivative: Efficacy in the Management of Pain, Neuropathy, and Inflammation Using In Vivo and In Silico Approaches. *ACS Omega* **2023**, *8* (25), 22809−22819.
(45) Cui, Y. R.; He, J. S.; Li, X. M.; Zhao, J. X.; Chen, A. L.; Yang, J. Preparation and characterization of MoS2 microsphere by hydrothermal method. *Adv. Mater. Res.* **2013**, *631*−*632*, 306−309.
(46) Xuan, T. T.; Long, L. N.; Van Khai, T. Effect of reaction temperature and reaction time on the structure and properties of MoS2 synthesized by hydrothermal method. *Vietnam J. Chem.* **2020**, *58* (1), 92−100.
(47) Liu, Y.; Peng, J.; Wang, S.; Xu, M.; Gao, M.; Xia, T.; Weng, J.; Xu, A.; Liu, S. Molybdenum disulfide/graphene oxide nanocomposites show favorable lung targeting and enhanced drug loading/tumor-killing efficacy with improved biocompatibility. *NPG Asia Mater.* **2018**, *10* (1), No. e458.
(48) Sari, F. N. I.; Ting, J. M. MoS_2/MoO_x-Nanostructure-Decorated Activated Carbon Cloth for Enhanced Supercapacitor Performance. *ChemSusChem* **2018**, *11* (5), 897−906.
(49) Liu, J.; Zeng, Z.; Cao, X.; Lu, G.; Wang, L. H.; Fan, Q. L.; Huang, W.; Zhang, H. Preparation of MoS(2)-polyvinylpyrrolidone nanocomposites for flexible nonvolatile rewritable memory devices with reduced graphene oxide electrodes. *Small* **2012**, *8* (22), 3517−3522.
(50) Khan, A. W.; Ali, J.; Kotta, S.; Ansari, S. H.; Sharma, R. K.; Kumar, A. Formulation development, optimization and evaluation of aloe vera gel for wound healing. *Pharmacogn Mag* **2013**, *9* (36), S6−S10.
(51) Arunbalaji, S.; Ismail, M. A. M.; Arivanandhan, M.; Alsalme, A.; Alghamdi, A.; Jayavel, R. High sensitive electrochemical nitrite sensor using Fe2O3/MoS2 nanocomposites synthesized by facile method. *Bull. Chem. Soc. Jpn.* **2020**, *93* (12), 1564−1570.
(52) Zhang, R.; Li, Y.; Qi, J.; Gao, D. Ferromagnetism in ultrathin MoS 2 nanosheets: from amorphous to crystalline. *Nanoscale Res. Lett.* **2014**, *9*, 586.
(53) Lalithambika, K. C.; Shanmugapriya, K.; Sriram, S. Photocatalytic activity of MoS 2 nanoparticles: an experimental and DFT analysis. *Appl. Phys. A: Mater. Sci. Process.* **2019**, *125*, 817.
(54) Feng, W.; Chen, L.; Qin, M.; Zhou, X.; Zhang, Q.; Miao, Y.; Qiu, K.; Zhang, Y.; He, C. Flower-like PEGylated MoS2 nanoflakes

https://doi.org/10.1021/acsomega.4c04252
ACS Omega 2024, 9, 37105−37116

for near-infrared photothermal cancer therapy. *Sci. Rep.* **2015**, *5* (1), 17422.
(55) Patzelt, A.; Richter, H.; Knorr, F.; Schafer, U.; Lehr, C. M.; Dahne, L.; Sterry, W.; Lademann, J. Selective follicular targeting by modification of the particle sizes. *J. Controlled Release* **2011**, *150* (1), 45−48.
(56) Liu, X.; Shen, B.; Shen, C.; Zhong, R.; Wang, X.; Yuan, H. Nanoparticle-loaded gels for topical delivery of nitrofurazone: Effect of particle size on skin permeation and retention. *J. Drug Delivery Sci. Technol.* **2018**, *45*, 367−372.
(57) Ganesan, P.; Soundararajan, R.; Shanmugam, U.; Ramu, V. Development, characterization and solubility enhancement of comparative dissolution study of second generation of solid dispersions and microspheres for poorly water soluble drug. *Asian J. Pharm. Sci.* **2015**, *10* (5), 433−441.
(58) Mulu, M.; RamaDevi, D.; Belachew, N.; Basavaiah, K. Hydrothermal green synthesis of MoS(2) nanosheets for pollution abatement and antifungal applications. *RSC Adv.* **2021**, *11* (40), 24536−24542.
(59) Tan, C.; Cao, X.; Wu, X. J.; He, Q.; Yang, J.; Zhang, X.; Chen, J.; Zhao, W.; Han, S.; Nam, G. H.; et al. Recent Advances in Ultrathin Two-Dimensional Nanomaterials. *Chem. Rev.* **2017**, *117* (9), 6225−6331.
(60) Wang, J.; Sui, L.; Huang, J.; Miao, L.; Nie, Y.; Wang, K.; Yang, Z.; Huang, Q.; Gong, X.; Nan, Y.; et al. MoS(2)-based nanocomposites for cancer diagnosis and therapy. *Bioact Mater.* **2021**, *6* (11), 4209−4242.
(61) Ismail, K. B. M.; Arun Kumar, M.; Mahalingam, S.; Kim, J.; Atchudan, R. Recent Advances in Molybdenum Disulfide and Its Nanocomposites for Energy Applications: Challenges and Development. *Materials* **2023**, *16* (12), 4471.
(62) Shen, C.; Shen, B.; Liu, X.; Yuan, H. Nanosuspensions based gel as delivery system of nitrofurazone for enhanced dermal bioavailability. *J. Drug Delivery Sci. Technol.* **2018**, *43*, 1−11.
(63) Shen, C.-y.; Xu, P.-h.; Shen, B.-d.; Min, H.-y.; Li, X.-r.; Han, J.; Yuan, H.-l. Nanogel for dermal application of the triterpenoids isolated from Ganoderma lucidum (GLT) for frostbite treatment. *Drug Delivery* **2016**, *23* (2), 610−618.
(64) Milanowski, B.; Wosicka-Frackowiak, H.; Glowka, E.; Sosnowska, M.; Wozny, S.; Stachowiak, F.; Suchenek, A.; Wilkowski, D. Optimization and Evaluation of the In Vitro Permeation Parameters of Topical Products with Non-Steroidal Anti-Inflammatory Drugs through Strat-M® Membrane. *Pharmaceutics* **2021**, *13* (8), 1305.
(65) Chatterjee, B.; Reddy, A.; Santra, M.; Khamanga, S. Amorphization of Drugs for Transdermal Delivery-a Recent Update. *Pharmaceutics* **2022**, *14* (5), 983.
(66) Sabbagh, F.; Muhamad, I. I. Acrylamide-based hydrogel drug delivery systems: Release of Acyclovir from MgO nanocomposite hydrogel. *J. Taiwan Inst. Chem. Eng.* **2017**, *72*, 182−193.
(67) Gooneh-Farahani, S.; Naghib, S. M.; Naimi-Jamal, M. R.; Seyfoori, A. A pH-sensitive nanocarrier based on BSA-stabilized graphene-chitosan nanocomposite for sustained and prolonged release of anticancer agents. *Sci. Rep.* **2021**, *11* (1), 17404.
(68) R Varges, P.; M Costa, C.; S Fonseca, B.; F Naccache, M.; De Souza Mendes, P. R. Rheological Characterization of Carbopol® Dispersions in Water and in Water/Glycerol Solutions. *Fluids* **2019**, *4* (1), 3.
(69) Gökçe, G.; Karavana, S. Y.; Bağriyanik, H. A.; Pekçetin, Ç.; Yapar, E. A.; Tural, G. A.; Gökçe, E. H. Design and in vitro, in vivo evaluation of antioxidant bioadhesive gels for burn treatment. *Turk. J. Biol.* **2022**, *46* (3), 251−262.
(70) Lino, C. S.; Taveira, M. L.; Viana, G. S. B.; Matos, F. J. A.; Plants, S. R. o.; Products, P. Analgesic and antiinflammatory activities of Justicia pectoralis Jacq and its main constituents: coumarin and umbelliferone. *Phytother. Res.* **1997**, *11* (3), 211−215.
(71) Mazimba, O. J. B. o. F. o. P. Umbelliferone: Sources, chemistry and bioactivities review. *Bull. Fac. Pharm. (Cairo Univ.)* **2017**, *55* (2), 223−232.
(72) Marto, J.; Baltazar, D.; Duarte, A.; Fernandes, A.; Gouveia, L.; Militao, M.; Salgado, A.; Simoes, S.; Oliveira, E.; Ribeiro, H. M. Topical gels of etofenamate: in vitro and in vivo evaluation. *Pharm. Dev. Technol.* **2015**, *20* (6), 710−715.

https://doi.org/10.1021/acsomega.4c04252
ACS Omega 2024, 9, 37105−37116